Quantification of the local magnetized nanotube *domains* accelerating the photocatalytic removal of the emerging pollutant tetracycline

Jiajie Yu[a,b], John Kiwi[a,*], Ivica Zivkovic[c], Henrik M. Rønnow[c], Tianhe Wang[b], Sami Rtimi[a,*]

[a] *Ecole Polytechnique Fédérale de Lausanne, EPFL-SB-ISIC-GPAO, Station 6, CH-1015, Lausanne, Switzerland*
[b] *Chemicobiology and Functional Materials Institute, Nanjing University of Science and Technology, Nanjing 210094, PR China*
[c] *Laboratory of Quantum Magnetism, EPFL-SB-IPHYS-LQMPH, Station 3, CH-1015 Lausanne, Switzerland*

ARTICLE INFO

ABSTRACT

Evidence is presented for the enhanced photodegradation of tetracycline (TC) by $Ag_xO/FeO_x/ZnO$ nanotubes (NTs) compared to Ag_xO/ZnO nanotubes under low-intensity solar light irradiation. A higher amount of the local magnetic *domains* with random orientation in the $Ag_xO/FeO_x/ZnO$ NTs lead to a faster TC-degradation. Fe introduces intra-gap states in the ZnO NTs facilitating the e-transport under light. The $Ag_xO/FeO_x/ZnO$ nanotubes were observed to present predominantly semiconductor behavior during the light induced TC-degradation. The nature of the interaction between non-polarized photos with the local domains due the addition of Fe is discussed. By X-ray photoelectron spectroscopy (XPS) redox reactions were observed on the nanotube surface NTs leading to the reactive oxygen radical species (ROS). The ROS-intermediates were identified by appropriate scavengers. Fast TC-degradation kinetics was attained by a catalyst with a composition AgOx(5.8%)FeOx(21.9%) ZnO (72.3%) as determined by X-ray fluorescence (XRF). A scheme for the interfacial charge transfer (IFCT) between the oxides on the nanotube surface is presented. Magnetized nanotubes present a practical potential in environmental cleaning avoiding the high cost separation of the catalyst from the reaction media at the end of the process

1. Introduction

Antibiotics like tetracycline (TC) are used to treat common diseases or prevent some types of bacterial infection, but their environmental side effects/residues raise a big concern since they lead to the disappearance of important species in the ecosystem. In addition, if TC is administered over long-times it leads to antibiotic resistance [1–4]. Residual TC is found in furtive emissions, in sludge, sewage, groundwater and even drinking water, owing to the insufficient removal in municipal waste-water treatment plants [5]. By advanced oxidation processes (AOPs) the degradation of TC has been reported on ZnO suspensions [6]. Nevertheless, these suspensions have to be separated and regenerated at the end of the process requiring, labor, time and reagents. Magnetically separable ZnO doped NTs are investigated in the present study to avoid these drawbacks. Several alternative approaches have been used to degrade TC such as ultrasonic extraction [7], adsorption [8] and photocatalytic degradation [9–12].

ZnO is a photocatalyst studied for environmental remediation due to its non-toxicity, low cost, high stability and widespread availability [13]. It is highly photo-stable and widely used in the electronic industry

and more recently in photocatalytic processes due to its high electron transfer rate [6,13,14]. However, ZnO has a wide band gap of ~3.30 eV, restricting its absorption to a very small percentage of the solar irradiation. To extend its absorbance into the visible region, ZnO has been doped by Cu, Ag, Fe, Au and Pt [15]. ZnO NTs are used in electronics and optics due to their high porosity, stability and large surface specific area [16–20]. Ag-doping of ZnO enhances significantly the ZnO absorption in the visible region. Ag acts as a trapping-site for the charges induced on the ZnO under light hindering charge recombination [21–24]. FeO_x extend the response of ZnO into the visible region. Magnetically separable nanotubes have been suggested for the degradation of pollutants [25–28]. ZnO doped with Ag- and Fe-ions have been reported to increase the pollutant degradation kinetics [16–29]. The preparation of $AgOx/Fe_3O_4$ nanocomposites with strong catalytic properties has been reported, but not on ZnO-nanotubes. This study addresses the preparation, evaluation, surface properties and performance of $Ag_xO/FeO_x/ZnO$ NTs leading to TC-degradation. To our knowledge, no study is available at the present time on magnetic $Ag_xO/FeO_x/ZnO$ nanotubes mediating TC-photodegradation. The way of intervention of these magnetic nanotubes under band-gap irradiation is

* Corresponding authors.
E-mail addresses: john.kiwi@epfl.ch (J. Kiwi), sami.rtimi@epfl.ch (S. Rtimi).

addressed in a detailed, systematic and comprehensive way during the course of this study.

2. Experimental section

2.1. Materials preparation

The synthesis of Zn-nanotubes (NTs) follows the protocols found in references [18,19]. A solution 200 mL of zinc nitrate (0.1 M) and 200 mL of hexamethylene-tetramine (HMT) were mixed under stirring. This solution was transferred into a 500 mL flask and refluxed at 90 °C. Ag_xO/ZnO NTs were prepared by a photochemical reduction method. 100 mg of ZnO NTs were added to 40 mL ethanol and 0.1 M $AgNO_3$ (Sigma Aldrich) was then added into the suspension under stirring. The dispersion was irradiated in the Suntest solar simulator for 2 h to drive the ethanol reduction of Ag^+ to $Ag°$. The suspension was then filtered, washed and dried before calcination at 500 °C for 1 h. Samples of ZnO NTs were also investigated in control runs. Therefore, due to the high calcination temperature used in the ZnO NTs synthesis a low BET area is expected for theses samples

The addition of Fe to the Ag_xO/ZnO NTs was carried out in 40 mL de-ionized water purged by N_2. Appropriate amounts of $FeCl_2·4H_2O$ (Sigma Aldrich) and $FeCl_3·6H_2O$ were added in the ratio $[Fe^{2+}]$: $[Fe^{3+}] = 1 : 2$. An aliquot of 1 mL of NH_3 (Merck, 25%) was added to 100 mg Ag_xO/ZnO nanotubes. A black precipitate was observed after stirring for 45 min at 85 °C. The precipitate was separated from the solution using a magnet and then washed repeatedly with deionized water and the precipitate was subsequently dried at 70 °C. The minimum weight ratio of $[Fe_{total}]$: $[Ag_xO/ZnO]$ required to induce magnetic properties on the photocatalyst was ~5%.

During this study the Ag_xO (15%)/FeO_x(20%)/ZnO was found to lead to the fastest TC-degradation. The percentages of the 3 oxides in the later compound refer to the reagents used in the composite preparation as described above in this section.

By reversing the order of the addition of Ag and Fe on the ZnO NTs, composites of $FeO_x/Ag_xO/ZnO$ were obtained and tested during the course of this study to pinpoint the intervention of each metal dopant in the NTs composite during the TC-degradation. The tetracycline (TC) formula is shown below:

$C_{22}H_{24}N_2O_8$

$C_{22}H_{24}N_2O_8$
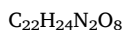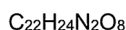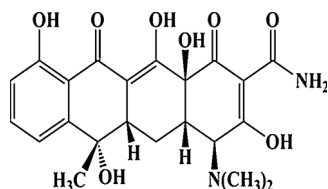
2.2. Photocatalytic degradation of tetracycline (TC) and irradiation procedures

The photocatalytic degradation of TC was carried out in the cavity of a Suntest solar simulator CPS (Atlas GmbH, Hanau, Germany). The effect of the light intensity on nanotube suspensions of ZnO, Ag_xO/ZnO, FeO_x/ZnO and $Ag_xO/FeO_x/ZnO$ mediating TC photo-degradation was carried out in a Suntest solar simulator. In a typical run, 25 mg of the selected catalyst was placed in a 50 mL photochemical reactor before adding 50 mg/L TC. The pH of the pollutant was adjusted by 0.1 M NaOH or 0.1 M HCl aqueous solutions. Prior to irradiation, the samples were equilibrated in the dark for 30 min. The TC-concentration was followed at 372 nm by UV–vis spectroscopy. At pre-selected times, 2 mL aliquots were withdrawn to monitor the TC-degradation kinetics. The

use of scavengers was employed to determine the specific role of leading to TC degradation. An aliquot of 1 mM p-benzoquninone was used to scavenge $HO_2^{-·}$ radical species; 1 mM NaN_3 to scavenge the singlet oxygen $^1O_2$; 1 mM methanol to scavenge the ·OH-radical and 1 mM EDTA-2Na to scavenge the valence band-holes (h+) [30]. The amount of the Fe(II) and Fe(III)-ions leached in solution and the absorbance of Fe(III) was followed by a Ferrozine in acetate buffer solution at 562 nm. Then, hydroxylamine-hydrochloride (10%w/w) was added in solution to reduce Fe^{3+} to Fe^{2+} and the absorbance of Fe^{2+} was measured again after 10 min at 562 nm.

2.3. Analytical methods

High pressure liquid chromatography (HPLC) was performed on an Agilent 1100 instrument equipped with a C18 column (Superlcosil LC-18, 5 µm particle size, length 15 cm, i.d. 3 mm) with UV detector (λ = 372 nm). 20 µL pollutant solution was injected into the HPLC with a mobile phase consisting of acetonitrile and 0.1% formic acid solution in a ratio of 20:80. The flow rate was set at 0.85 mL/min (25 °C). The removal of TOC was monitored by a Shimadzu TOC-V CSH analyzer.

2.4. Surface characterization of the NTs

By X-ray fluorescence (XRF) the surface weight percentage of the NTs composites was determined. The data is presented in Table 1. The faster TC-degradation kinetics was attained by a catalyst with a composition $Ag_xO(5.8\%)/FeO_x(21.9\%)/ZnO(72.35\%)$. The X-ray diffraction (XRD) measurements were registered in an X'Pert MPD PRO from PANalytical equipped with a secondary graphite (002) monochromator and an X'Celerator detector operated in Bragg-Brentano geometry. The surface atomic percentage concentration of Zn, Ag and Fe in the uppermost 10 layers (2 nm) of the nanotubes was determined by X-ray photoelectron spectroscopy (XPS). An AXIS NOVA photoelectron spectrometer (Kratos Analytical, Manchester, UK) provided for with monochromatic AlK_α(hν = 1486.6 eV) anode. Binding energies (BE) were calibrated against the standard C1s binding energy at 284.8 eV [31,32]. Spectra were deconvoluted by means of a Multipak (version 9 software) using 50:50 Gaussian: Lorentzian peak shape and a Shirley background function [33]. The magnetic measurements on the composite catalysts were performed with a Quantum Design NPMS-Xl 5T superconducting interference device (SQUID) magnetometer. The magnetic powder samples were mixed with a diluted GE-varnish and measured at 300 K in the field-sweep sequence 0 T → 5 T → -5 T → 5 T.

3. Results and discussions

3.1. Photodegradation of TC and optimization of the parameters leading to TC-mineralization

Fig. 1a shows that the runs mediated by Ag_xO (15%)/FeO_x(20%)/ ZnO NTs lead to a TC-photo-degradation of ~85% within 240 min compared to the slower TC photo-degradation by ZnO, Ag_xO (15%)/ ZnO and FeO_x/ZnO NTs. The rate constant of $Ag_xO(15\%)/FeO_x(20\%)/$ ZnO was 0.0115 min^{-1}. This is 1.83 times higher compared to the rate observed on bare ZnO (0.0063 min^{-1}). The TC-degradation observed in the dark was due to the TC-adsorption and the effect of Ag in the Ag_xO

Table 1
Weight percentage of the Ag, Fe and Zn elements determined by X-ray fluorescence (XRF) for different composite nanotubes.

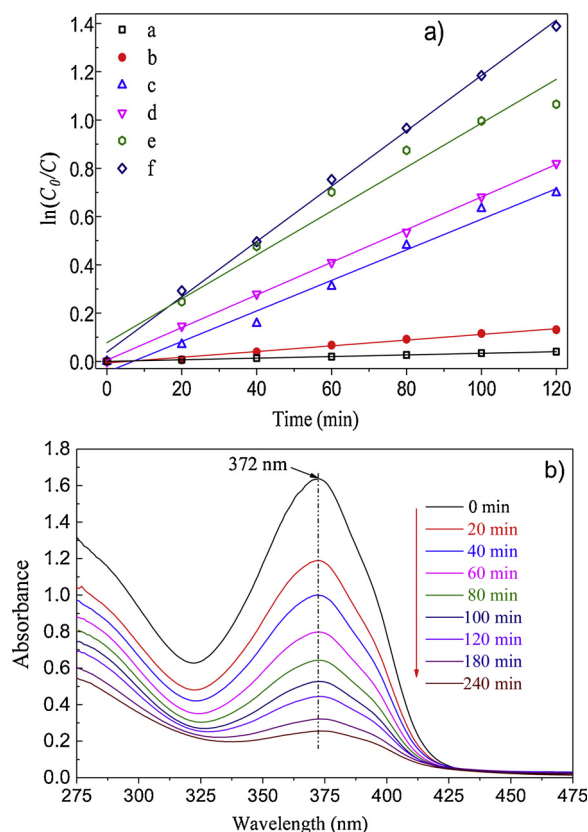| Sample	Ag	Fe	Zn
$FeO_x(20\%)/ZnO$		0.292	0.708
$Ag_xO(15\%)/ZnO$	0.080		0.920
$Ag_xO(15\%)/FeO_x(20\%)/ZnO$	0.058	0.219	0.723

Fig. 1. (a) $\ln(C_0/C)$ data as a function of time for different catalysts during the degradation of TC, under simulated solar light: (a) photolysis of TC no catalyst added, (b) $Ag_xO(15\%)/FeO_x/(20\%)/ZnO$, dark c) FeO_x, light, d) ZnO, light, e) $Ag_xO(15\%)/ZnO$, $FeO_x(20\%)/ZnO$ light, f) $Ag_xO(15\%)/FeO_x(20\%)/ZnO$ under sunlight irradiation. (b) time-dependent UV–vis absorption spectra of TC degraded by way of $Ag_xO(15\%)/FeOx(20\%)/ZnO$. Solution parameters: [catalyst] = 500 mg/L, [TC] = 50 mg/L, pH = 7 and simulated solar light intensity = 44.6 mW/cm^2.

(15%)/FeO$_x$(20%)/ZnO and was of the order of 15.4%.

Catalysts containing Ag$_x$O on ZnO followed by the deposition of FeO$_x$ led to a TC-photodegradation kinetics similar to the one observed when FeO$_x$ was deposited first followed in a second stage by the deposition of Ag$_x$O on ZnO. This suggests that the catalyst calcination at 500 °C induces FeO$_x$ and Ag$_x$O NPs deeply buried states in the bulk of the ZnO-network. The e-/h + charges generated on the ZnO will then not preferentially interact with these FeO$_x$ or Ag$_x$O deep sites bur react with closer O$_2$(air) and the $Zn-OH$ surface groups leading to reactive oxygen intermediates (ROS). The decrease in the TC-main absorption peak at 372 nm within the photo-degradation time was followed up to 4 h in the solar simulator cavity as shown in Fig. 1b.

Fig. 2 shows the high-pressure liquid chromatography (HPLC) data observed during TC-degradation mediated by Ag$_x$O(15%)/FeO$_x$(20%)/ZnO nanotubes. The retention time of ~6.2 min decreased within the degradation time (240 min). This is consistent with the data reported during the TC-degradation by UV–vis spectroscopy in Fig. 1. No additional peaks appeared within the TC-degradation time in the HPLC-spectrogram, indicating that no long-lived degradation intermediates were generated during TC-degradation. Supplemental

Total organic carbon (TOC) was used to evaluate the TC mineralization kinetics mediated by Ag$_x$O(15%)/FeO$_x$(20%)/ZnO under solar light irradiation and the results are shown in Fig. 3. About 56.8% of TOC was removed on Ag$_x$O(15%)/FeO$_x$(20%)/ZnO NTs while only 46.4%, 49.3%, 50.2% removal was observed on bare ZnO, FeO$_x$(20%)/ ZnO and Ag$_x$O (15%)/ZnO. The TOC 56.8% reduction of TC is higher compared to TC-degradation results reported elsewhere [31–33]. The

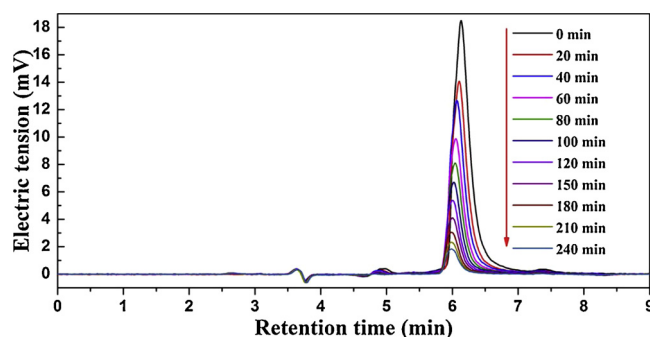**Fig. 2.** High Pressure liquid chromatography (HPLC) spectra of TC degradation with time on Ag$_x$O(15%)/FeO$_x$(20%)/ZnO. Solution parameters: [catalyst] = 500 mg/L, [TC] = 50 mg/L, pH = 7 and light intensity = 44.6 mW/cm^2.
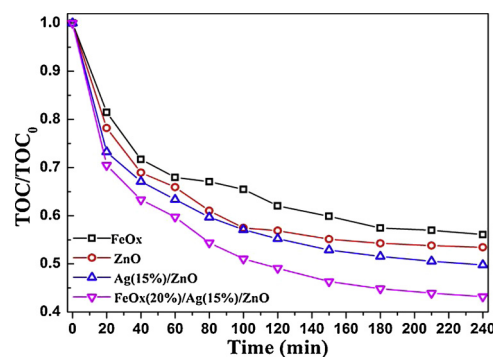

Fig. 3. Total organic carbon decrease from TC with time over different photocatalysts under simulated solar light on (1) Ag$_x$O(15%)/FeO$_x$(20%)/ZnO, (2) Ag$_x$O(15%)/ZnO, (3) ZnO and (4) FeO$_x$. Solution parameters: [catalyst] = 500 mg/L, [TC] = 50 mg/L, pH = 7 and light intensity = 44.6 mW/cm^2.

data in Fig. 3 shows that at an initial pH 7.0, TC was not fully mineralized. This is due to long-lived intermediates formed in solution resistant to the attack of the photo-generated ROS and of the ZnOvb-holes. No specific identification of the TC-residuals of the residuals was carried out to see whether the residuals of TC-degradation were toxic or not. This topic may be addressed in a separate study, but it is beyond the scope and objectives of the present study.

Supplemental Figure S1 shows the shifts of TC-peak due to the presence of ZnO, FeO$_x$(20%)/ZnO, Ag$_x$O(15%)/ZnO and Ag$_x$O(15%)/ FeO$_x$(20%)/ZnO in the dark for 30 min at 356 nm, 364 nm, 372 nm and 374 nm respectively. A spectral shift was not observed in the presence of bare FeOx, which suggests that the red shift was caused by the interaction between TC and the ZnO NTs. The logarithmic (C$_0$/C) plot of the TC pseudo first-order TC-photodegradation on ZnO NTs heated at different times is reported in the Supplemental Figure S2. The data shows that heating for 72 h led to the most suitable degradation kinetics. Supplementary Figure S3 shows that Ag$_x$O of 15% added to the ZnO nanotubes led to the fastest TC photo-degradation. The 15% limit is due to the Ag filtering the light reaching the ZnO NTs [34]. Silver has been reported to increase the ZnO photocatalytic activity due to its visible light absorption. It also furthers the separation of the e-/h + pairs in ZnO introducing surface plasmon resonance [35–37]. Supplementary Figure S4 shows that an increase in the FeOx in the ZnO NTs surface lead to 20% faster TC-removal kinetics. Figure S5 shows the HPLC-signal for TC presenting a low peak symmetry. Interestingly enough, the TC-peak symmetry was improved during the TC-degradation mediated by Ag$_x$O(15%)/FeO$_x$(20%)/ZnO probably due to the increased TC-adsorption on the photocatalyst surface.

The FeOx absorbs visible light up to 535 nm. This is within the range of the Fe$_2$O$_3$ band-gap (2.2 eV) [38,39] promoting the cbe- from the Fe$_2$O$_3$vb to the Fe$_2$O$_3$cb. By XPS the Fe$_2$O$_3$ signals were identified as

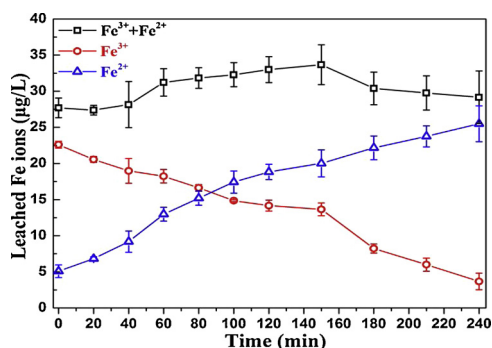**Fig. 4.** Determination of Fe-ions leaching from $Ag_xO(15\%)/FeO_x(20\%)/ZnO$ during the photodegradation of TC. Solution parameters: [catalyst] = 500 mg/L, [TC] = 50 mg/L, pH = 7 and light intensity = 44.6 mW/cm^2.

shown below in Section 3.3. The potential energy of ZnOcb is known to be more cathodic respect to the one of iron oxide and the ZnOvb is more anodic compared to the one in Fe_2O_3. Therefore, the migration from Fe_2O_3 to ZnO is not thermodynamically feasible but light absorption by $FeOx/Fe_2O_3$ accelerates the TC degradation as shown in Fig. 1a, trace e).

The total concentration of Fe-ions (Fe^{2+} + Fe^{3+}) was 33–34 micrograms/L within 150 min as shown in Fig. 4. The initial concentration of Fe^{3+}-ions was higher compared to the Fe^{2+}-ions in solution. Fig. 4 shows the amount of leached Fe^{3+} and Fe^{2+}- as a function of the reaction time. The reaction rate of Fe^{3+} to Fe^{2+} (k_1 = 76 $M^{-1}S^{-1}$) is faster compared to the reaction rate of Fe^{2+} to Fe^{3+} (k_2 = 0.02 $M^{-1}S^{-1}$) [40,41].

The stability of $Ag_xO(15\%)/FeO_x(20\%)/ZnO$ was evaluated by its reusability during TC-degradation and the data is shown in Fig. 5. After each degradation cycle, the catalyst was separated from the solution by way of an external magnet. The catalyst was washed after each cycle with de-ionized water and ethanol and dried at 70 °C for 1 h. Fig. 5 shows the photo-degradation of TC attaining ~80% pollutant removal (86% TC removal was observed during the first degradation cycle as shown in Fig. 5). The stability of the catalyst used in the repetitive TC-degradation was further investigated by following quantitatively the leaching of the Fe-ions during TC-degradation by the Ferrozine method [40]. In general, the deposition of non-mineralized residuals on a catalyst surface partly hinders the close contact with the pollutant. This poisons the heterogeneous photocatalytic degradation of pollutants and consequently reduces the operational lifetime of the catalyst [10,11,13].
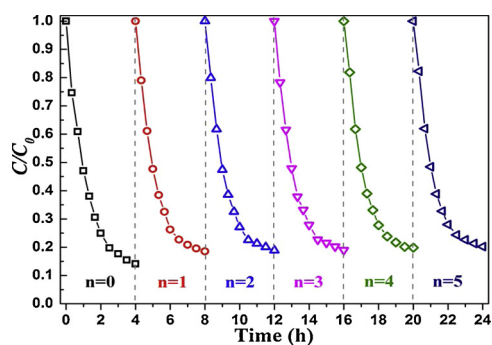

Fig. 5. Five consecutive photodegradation TC-cycles over $Ag_xO(15\%)/FeO_x(20\%)/ZnO$. Solution parameters: [catalyst] = 500 mg/L, [TC] = 50 mg/L, pH = 7 and light intensity = 44.6 mW/cm^2.
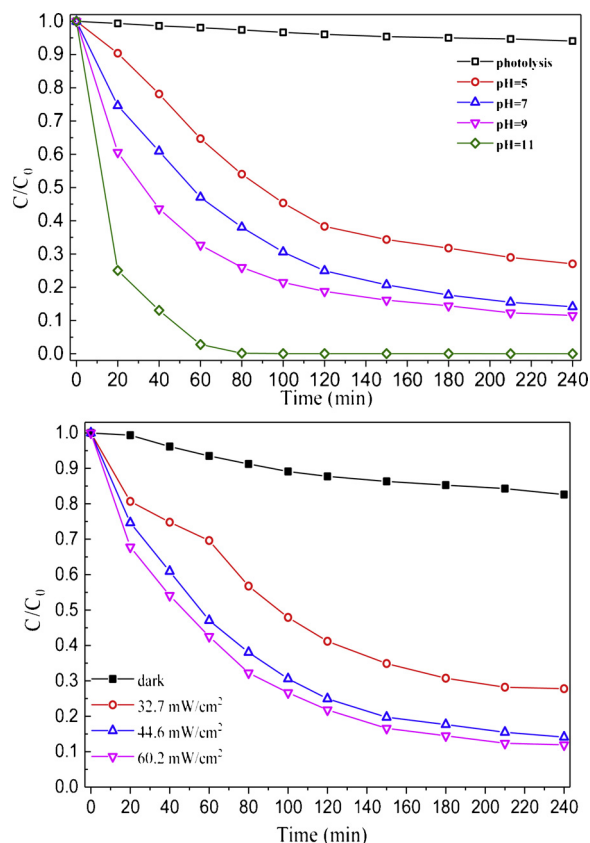

Fig. 6. (a) TC-photodegradation as a function of solution pH and (b) as a function of light intensity. Solution parameters [catalyst] = 500 mg/L, [TC] = 50 mg/L and pH = 7) during the TC-degradation mediated by Ag_xO (15%)/$FeO_x(20\%)/ZnO$ NTs. Solution parameters [catalyst] = 500 mg/L, [TC] = 50 mg/L and light intensity = 44.6 mW/cm^2).

3.2. Effects of the initial catalyst concentration, TC-concentration, solution pH, light intensity and radical intermediates intervening during the TC-removal

Fig. 6a presents the results of TC-photodegradation as a function of solution pH in the range 5 up to 11. It is readily seen that at more alkaline pH-values, the TC-removal becomes faster. The TC was removed completely at pH 11 within 80 min on the $Ag_xO(15\%)/FeO_x(20\%)/ZnO$ NTs while only ~63% was degraded at pH 5.

ZnO is an amphoteric material with a high isoelectric point (IEP) of ~9.5. It will interact electrostatically with the TC peripheral functional groups showing a pK'a < 9.5 [42,43]. TC presents pKa values at 3.3, 7.7, 9.7 and 12 giving raise to H_4TC^+, H_3TC, H_2TC and HTC^{2-} respectively [44]. Therefore, the H_3TC and HTC^{-2} will interact electrostatically with the $ZnOH_2^+$ in the solution at pH < 9.5. At pH 11, the TC form HTC^{2-} is negatively charged and the ZnO- undergoes an electrostatic repulsion with HTC^{2-}. However, at pH 11, the concentration of ·OH in the solution at this alkaline pH is high. The HTC^{2-} negatively charged TC attracts the electrophilic ·OH due to the high TC-ring charge density. These later two factors may account for the fast TC-degradation at pH 11 as shown in Fig. 6a. The TC-peripheric functional groups: -C; -C=O and NH- interacting with Zn/ZnO are shown below in Scheme 1:

Fig. 6b shows the effect the light intensity on TC-degradation mediated by $Ag_xO(15\%)/FeO_x(20\%)/ZnO$. As the light intensity is increased, the TC-degradation became faster. This is the evidence for an increased charge separation in ZnO at higher light doses. Therefore, the semiconductor behavior of the ZnO predominates in the TC-degradation kinetics over the effect due to the highly oxidative metal and oxides
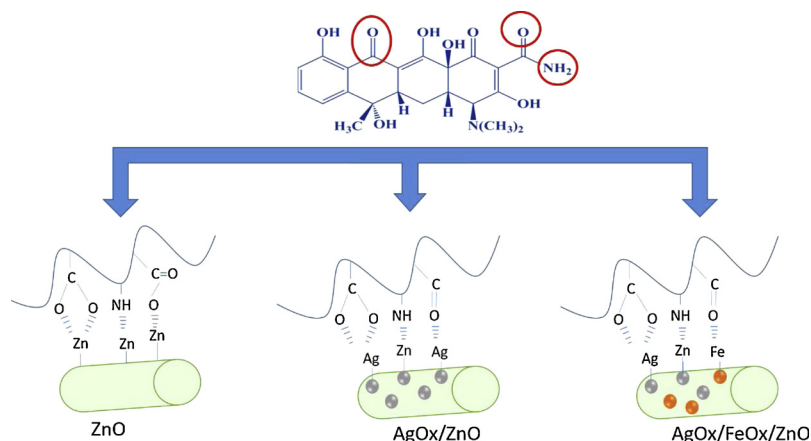
Scheme 1. TC functional groups coordination groups with ZnO, Ag_xO/ZnO and Ag_xO/FeO_x/ZnO.

Ag_xO and FeO_x.

The supplemental Figure S6a shows the beneficial effect the increased catalyst concentration up to 1 g/L on the TC-degradation kinetics due to the increased amount of catalytic sites introduced in the suspensions at higher Ag_xO/(15%)/FeO_x(20%)/ZnO concentrations. Figure S6b shows a slower TC-degradation kinetics due to a higher TC-concentration, a feature characteristic of heterogeneous catalytic reactions.

It is well known that reactive oxygen species (ROS) such as OH, $^1O_2$, O_2^-.and vbh^+ play an important role in the photo-degradation of organic pollutants [30,35–37]. To identify the ROS, appropriate radical-scavengers such as methanol (OH scavenger), p-benzoquinone ($^.O_2^-$ scavenger), NaN_3 ($^1O_2$) and disodium ethylene-diamine-tetra-acetate dehydrate (EDTA-2Na, holes scavenger) were used in the present study and the data is presented in Fig. 7 [45]. The degradation rate of TC decreased from ~86% to ~47% upon addition of p-benzoquinone, an O_2^-. scavenger showing that $^.O_2^-$ was the main intermediate leading to TC-degradation [30,45]. The pH of the TC-solution was observed to decrease from 7.32 to 7.05 after 4 h irradiation. This corresponds to more than a twofold increase in the solution H^+-concentration as shown in reaction (1) since the TC-degradation was carried out at pH > 4.8

$$HO_2^° \Leftrightarrow O_2^{°-} + H^+ \quad pK_a \ 4.8 \tag{1}$$
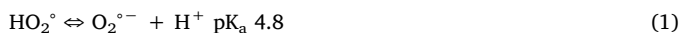
Other ROS-species as shown in Fig. 7 decreased the TC-degradation up to 10% and were therefore of secondary importance during the TC-degradation.
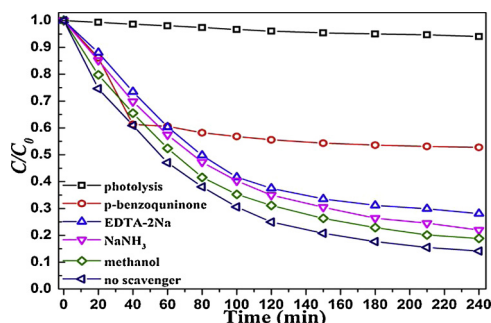

Fig. 7. Tetracycline degradation on Ag_xO(15%)/FeO_x(20%)/ZnO in the presence of: 1 mM p-benzoquinone, 1 mM NaN_3, 1 mM methanol, 1 mM EDTA-2Na and no scavenger. Solution parameters: [TC] = 50 mg/L, pH = 7 and light intensity = 44.6 mW/cm^2.

3.3. Physical characterization of the catalyst surfaces by X-Ray diffraction (XRD) and X-ray photoelectron spectroscopy (XPS)

Fig. 8a presents the XRD data for the different NTs investigated during the course of this study. The XRD peaks of ZnO NTs were indexed and correspond to the wurtzite hexagonal phases of ZnO (JCPDS card No.36–1451). No additional crystalline ZnO-phases were detected. The intensities of the ZnO diffraction peaks in FeO_x(20%)/ZnO, Ag_xO (15%)/ZnO and Ag_xO(15%)/FeO_x(20%)/ZnO were seen to decrease upon incorporation of Fe or Ag-oxides leading to lower ZnO XRD signals. The FeO_x peaks at 30.28°, 35.68° and 62.94° of maghemite (JCPDS card No.25–1402) were not noticeable in the FeO_x(20%)/ZnO and Ag_xO (15%)/FeO_x(20%)/ZnO composites. The amount of FeO_x was too small and therefore beyond the XRD detection limit. The peaks in Ag_xO (15%)/ZnO at 2Θ = 38.11°, 44.30° and 64.44° were assigned to Ag° and Ag_2O. This is consistent with XPS observations addressed in the paragraph below. By way of the Debye-Scherrer equation [46] it was possible to estimate a crystallite size for FeOx using the (119) reflections. The sizes of silver at time zero in Ag_xO(15%)/ZnO and in Ag_xO(15%)/ FeO_x(20%)/ZnO were found to be 26.55 nm and 23.82 nm, respectively. Table 2 shows the crystallite sizes for ZnO, Ag_xO and FeO_x. The reduction in the silver size in Ag_xO(15%)FeO_x(20%)/ZnO was probably due its increase in compactness during the annealing of the Fe_xO/ZnO composite. Fig. 8b shows the XRD spectrogram of Ag_xO(15%)/ FeO_x(20%)/ZnO before and after 5 cycles. The intensity of the peaks on Fig. 8b were similar before and after the catalyst reuse. This provides a further proof of the catalytic stability of the Ag_xO(15%)/FeO_x(20%)/ ZnO NTs composites during cyclic TC-photodegradation.

The chemical states of Fe and Ag in the Ag_xO(15%)/FeO_x(20%)/ ZnO before and after TC-degradation were determined by X-ray photoelectron spectroscopy (XPS). For convenience Ag_xO(15%)/ FeO_x(20%)/ZnO was written as Ag_yO(15%)/FeOx(20%)/ZnO in the XPS-section. Fig. 9a shows the survey XPS-spectrum of Ag_yO(15%)/ FeOx(20%)/ZnO before and after TC-degradation. Zn, O, Ag and Fe are the major elements detected on Ag_xO(15%)/FeO_x(20%)/ZnO. Fig. 9b shows peaks at a BE 1044.7 eV and 1021.6 eV for Zn 2p3/2 and Zn 2p1/ 2 [49]. These were reduced by 20% after the sample reuse. The O1s spectra of Ag_xO(15%)/FeO_x(20%)/ZnO in Fig. 9c was deconvoluted into three peaks centered at 533.7 eV, 531.7 eV and 530.1 eV corresponding to the loosely bonded O−H, O^{2-} in the oxygen deficient regions of ZnO wurtzite matrix comprising hexagonal a Zn^{2+}-ion array [47,48]. The reused Ag_yO(15%)/FeO_x(20%)/ZnO showed an increased O−H peak due to water chemisorption. Fig. 9d shows the XPS spectra of Ag for Ag_yO(15%)/FeO_x(20%)/ZnO at time zero with Ag peaks at BE 373.9 eV, 368.0 eV and 367.7 eV. These peaks were assigned to Ag_2O, Ag° and Ag_2O, respectively. Ag_2O is the major component Ag_yO(15%)/ FeO_x(20%)/ZnO. According to the fitting result of Ag 3d, the atomic
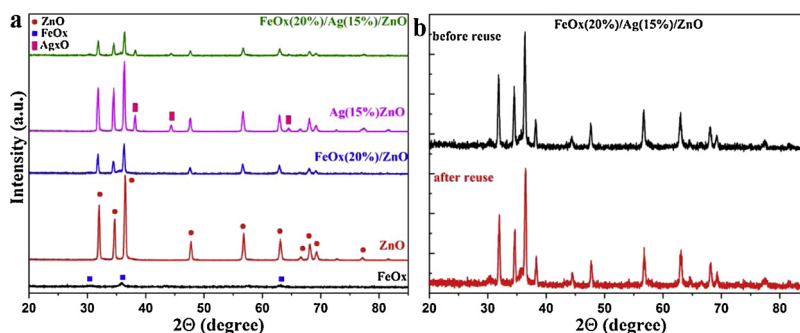
Fig. 8. (a) XRD patterns for the most relevant photocatalysts as noted in the Figure captions; (b) XRD of the $Ag_xO(15\%)/FeO_x(20\%)/ZnO$ photocatalyst before and after five recycling.

Table 2
Average crystallite size determined by X-Ray diffraction (XRD) for the oxides of photocatalysts samples calculated from the strongest peak signal.

Sample	ZnO (nm)	Ag₂O (nm)	Fe₂O₃ (nm)
FeOₓ			8.45
ZnO	28.58		
FeOₓ(20%)/ZnO	19.95		
AgₓO(15%)/ZnO	18.11	26.55	
AgₓO(15%)/FeOₓ(20%)/ZnO (before reuse)	23.82	23.82	
AgₓO(15%)/FeOₓ(20%)/ZnO (after reuse)	21.65	19.88	

ratio of $Ag^+/Ag°$ was found to be 2.3:1. The "y" value in $Ag_yO(15\%)/FeO_x(20\%)/ZnO$ was calculated to be 2.87. An additional Ag peak at BE 374 eV appear after recycling the sample five times. The atomic ratio of $Ag^+:Ag°$ in reused $Ag_yO(15\%)/FeO_x(20\%)/ZnO$ was 1.4 and the y-value then changed into 3.43. Ag_2O decomposes to $Ag°$ and AgO under light. AgO is not stable at room temperature and photo-reduces to $Ag°$ and O_2 [50]. The Fe3d XPS spectra of $Ag_yO(15\%)/FeO_x(20\%)/ZnO$ before and after reuse was shown in Fig. 10e. The main peak positions for Ag3d and Fe2p are shown in Table 2. Iron comprises two oxidation states, Fe^{2+} and Fe^{3+}, the former octahedral coordinated and the latter distributed over both octahedral (oct) and tetrahedral (tet) sites. At time zero, the sample BE was 709.9 eV due to Fe^{2+} (oct) species, with a satellite (sat) peak at 716.8 eV. The peaks at 710.8 eV and 713.4 eV correspond to the Fe (oct) and Fe (tet) species, with a corresponding satellite at 719.1 [32]. The Fe^{3+}/Fe^{2+} ratio was estimated to be 14.3: 1 for the Fe $2p_{3/2}$ transition, indicating that FeO_x was mainly Fe_2O_3. The x-value obtained for $Ag_yO(15\%)/FeO_x(20\%)/ZnO$ was 1.47. For the reused $Ag_yO(15\%)/FeO_x(20\%)/ZnO$ composite, the Fe^{3+}/Fe^{2+} ratio decreased to 3.9 : 1 and the x value became 1.40. This suggests redox catalysis taking place during the TC-degradation since different ratios of Fe^{3+}/Fe^{2+} were found on the catalyst surface before and after TC-degradation (Table 3).

3.4. Effect of the small magnetic domains due to the Fe-addition on the NTs

Fig. 10 presents the $FeO_x(20\%)/ZnO$ and $Ag_xO(15\%)/FeO_x(20\%)/ZnO$ samples presenting S-shaped magnetization loops. Fig. 10 shows the ZnO and $Ag_xO(15\%)/ZnO$ non-magnetic samples. The $Ag_xO(15\%)/FeO_x(20\%)/ZnO$ magnetization in Fig. 10 was slightly above the one found for the $FeOx(20\%)/ZnO$ sample. This correlates with the results presented in Fig. 1a, where the TC-degradation kinetics was faster for the sample shown in Fig. 1, trace f) compared to the sample Fig. 1, trace e). In Section 3.1, we have suggested the formation of FeO_x buried in ZnO and lead to the formation of Zn-O-Fe bonds. The ZnO protects the FeO_x NPs in the $Ag_xO(15\%)/FeO_x(20\%)/ZnO$ from corrosion. This seems to stabilize the FeO_x recycling of the composite catalyst during TC-degradation. The FeO_x/Fe_2O_3 in the sample would not be in contact with O_2(air) as noted in Section 3.1. Its addition to the $Ag_xO(15\%)/$ $FeO_x(20\%)/ZnO$ lead to the increased sample optical absorption as shown in Fig. 1, trace e). The addition of Fe to the ZnO NTs is responsible for the FeO_x intra-gap states formation in these samples as shown below in Fig. 11. The magnetic properties induced by these Fe magnetic intra-gap states increasing the performance for semiconductor mediated pollutant degradation present a potential practical application of $Ag_xO(15\%)/FeO_x(20\%)/ZnO$ composites.

3.5. Mode of intervention of the magnetic domains in the nanotubes during the photocatalysis

The $Ag_xO(15\%)/FeO_x(20\%)/ZnO$ sample in Fig. 1, trace f) is exposed to the hybrid light-wave and the FeO_x magnetic *domains* with random local orientation. The non-polarized incoming light reaches the $Ag_xO(15\%)/FeO_x(20\%)/ZnO$ NTs and interacts with the atomic and subatomic catalyst components. The interaction of the light with the subatomic short-lived excitons, bosons, quarks, mesons making up the atoms has been suggested to proceed at a speed higher compared to the speed of light [51,52]. Photons arriving on the NTs affect the electron distribution in the atomic and subatomic particles [51,52]. The addition of Fe- in the composite does not lead to any net nanotube magnetization. The local domains in the nanotubes due to added Fe acquire a small random magnetization in random directions but add to zero total magnetization. However, Fe-addition led to an increase of the oscillations in the metal/oxide electrons accompanied by heat effects.

The light wave will tunnel towards TC with a modified coherence due to the FeOx intra-gap states in $Ag_xO(15\%)/FeO_x(/20\%)/ZnO$ NTs. This introduces a significant modification of the magnetic field generated by the FeOx intra-gap states. The charge transfer from the major component ZnO to Ag_xO and FeO_x component will take place by way of quantum tunneling under the condition of work function equalization (or chemical potential equalization) between the composite oxides during the photocatalysis. This involves interfacial charge transfer and band bending between the oxide components of the composite catalyst.

The magnetic domains due to the addition of intra-gap FeO_x generate within the NTs generate small microampere currents since the nanotubes find themselves in aqueous media that is an excellent electrons conductor. FeO_x intra-gap states introduce inter-band states that accelerate the electron transfer from the valence band to the conduction band. This in turn accelerates the TC-degradation as reported in Fig. 1, trace f). The combined effect of light and magnetic field is related closer with quanta effects invoked by Bohr [53] than with the view suggested by Einstein [54]. Semiconductors with a band-gap > 2 eV in the presence of FeOx have been reported to present a modified electron heterostructure distribution with respect to ZnO [55].

The electro-neutrality in the ZnO network upon Fe-doping leads to the formation of oxygen vacancies. The number of vacancies would be less than the Fe^{3+}-cations incorporated at the Zn^{2+} sites as suggested in Eq. (2):
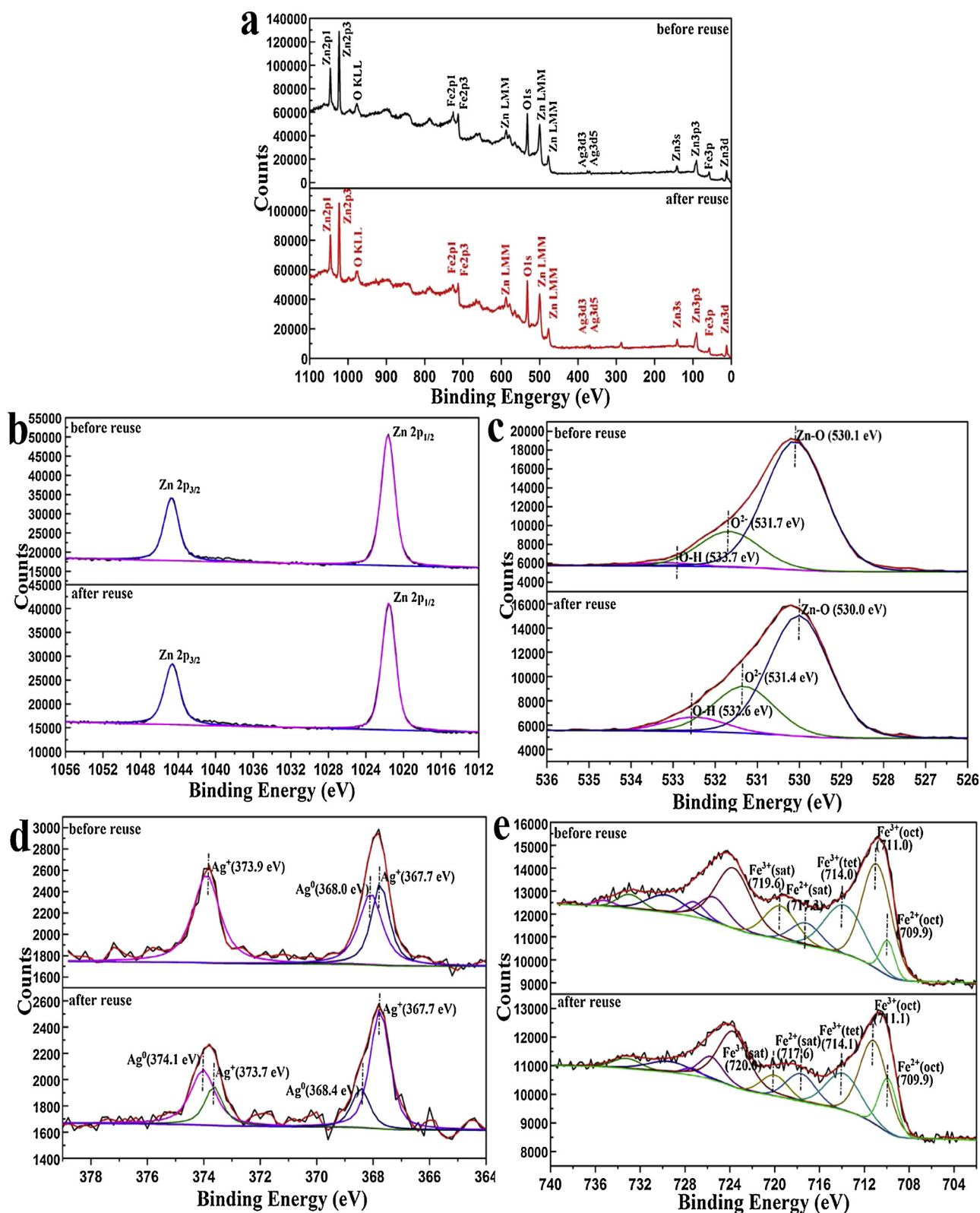
$$Fe_2O_3 \rightarrow Fe_{Zn} + V_{Zn}^{2/} + Oo \qquad (2)$$

Fig. 9. (a) X-ray photoelectron spectroscopy (XPS) survey spectra of $Ag_xO(15\%)/FeO_x(20\%)/ZnO$ before and after reuse, (b) Zn2p spectra before and after reuse, (c) O1s spectra before and after reuse, (d) Ag3d spectra before and after reuse, (e) Fe3d spectra before and after reuse.

where $V_{Zn}^{2/}$ refer to the cation vacancies (good h^+ acceptors), Fe_{Zn} are sites with good electron-acceptor properties. The sites that can interact with an electron leading to a $V_{Zn}^{1/}$-state in the ZnO band-gap and to O-atom in the ZnO lattice [55–57]. This description is consistent with the studies addressing: a) electrostatic interactions during the photocatalysis and b) the incoming light effect polarizing the atoms/subatomic particles in the catalyst [55–57].
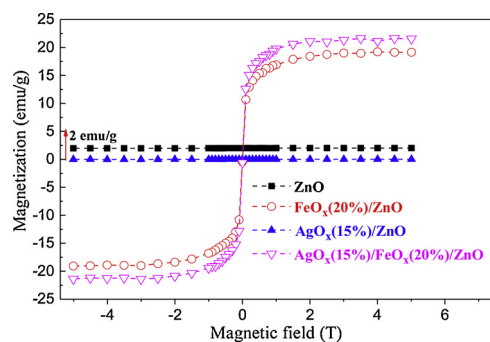
Fig. 10. Magnetization loops of the most relevant photocatalyst NTs intervening in the TC-degradation.

Table 3
XPS deconvolution of Ag 3d and Fe 2p from $Ag_xO(15\%)/FeO_x(20\%)/ZnO$ before and after TC-degradation.

| Species		Binding Energy (BE) before reuse	Binding Energy (BE) after reuse
Ag 3d	Ag 3d3/2	/	Ag° at 374.1 eV
		Ag^+ at 373.9 eV	Ag^+ at 373.7 eV
	Ag 3d5/2	Ag° at 368.4 eV	Ag° at 368.4 eV
		Ag^+ at 367.7 eV	Ag^+ at 367.7 eV
Fe 2p	Satellite	Fe^{3+} (sat) at 719.6 eV	Fe^{3+} (sat) at 720.0 eV
		Fe^{2+} (sat) at 717.3 eV	Fe^{2+} (sat) at 717.6 eV
	Fe 2p3/2	Fe^{3+} (tet) at 714.0 eV	Fe^{3+} (tet) at 714.1 eV
		Fe^{3+} (oct) at 711.0 eV	Fe^{3+} (oct) at 711.1 eV
		Fe^{2+} (oct) at 709.9 eV	Fe^{2+} (oct) at 709.9 eV
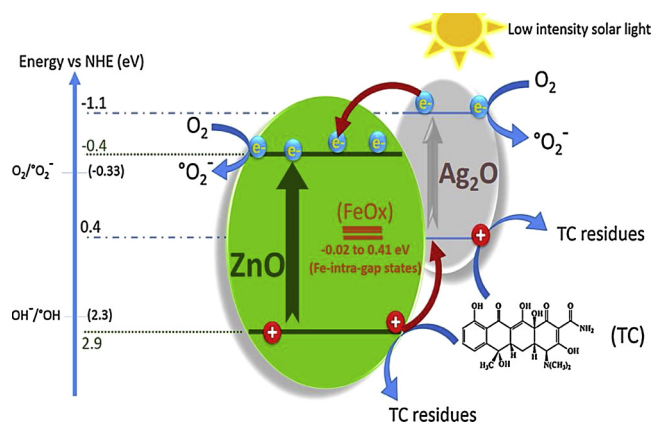
Fig. 11. Interfacial charge transfer mechanism leading to TC-degradation on $Ag_xO(15\%)/FeO_x(20\%)/ZnO$ under simulated solar light. The FeO_x presence is noted in the form of Fe-intra-gap states.

3.6. Interfacial charge transfer (IFCT) in the $Ag_xO(15\%)/FeO_x(20\%)/ZnO$ sample leading to TC-degradation: Mechanistic features

Based on the experimental result described in Sections 3.1-3.4, an interfacial charge transfer (IFCT) mechanism is suggested in Fig. 11.

In Section 3.3, Ag_2O was shown to be the major Ag-specie in the $Ag_xO(15\%)/FeO_x(20\%)/ZnO$ composite. By contact with the ZnO semiconductor, the Ag_2O acts as an effective metal conductor transferring the electrons generated by the ZnO under light into the aqueous solution. The NTs are in an aqueous media that is a very powerful electrical conductor.

The heterojunction between ZnO and Ag_2O promotes the charge transfer from the Ag_2Ocb to ZnOcb [58]. The different pace of the electron and hole photo-production rates leads to the accumulation of charges in their respective electronic bands increasing the rate of electron-hole recombination and slowing down TC photo-degradation.

The cbe- of ZnO and Ag_2O undergo cross-reactions with the vbh$^+$ of the second oxide present in the composite oxide decreasing the charge separation in each semiconductor [59]. The O_2-reduction induced by the cbe- of Ag_2O and ZnO lead to the production of the ROS-species since the cb potentials of ZnO and Ag_2O are more negative relative the reduction potential O_2/O_2^- (-0.16 eV vs NHE).

This allows the O_2 reduction leading to ROS-species as noted in Fig. 11 [60].

$$O_2 + e^- \rightarrow O_2\text{-} \tag{3}$$

$$O_2 + H^+ \rightarrow HO_2^-\cdot \tag{4}$$

Fig. 11, shows the role of the photogenerated electrons in Ag_2O and ZnO mediating TC-degradation under solar light. The reduction of O_2 by electrons noted in eq(3) is followed the reaction of $O_2^- + H^+ \rightarrow$ leading to highly oxidative radicals $HO_2\cdot$- and OH-radicals in aqueous solution. Evidence for this was presented in Fig. 7 (Section 3.2). The $HO_2\cdot$- species found by scavenging experiments appeared as the most important intermediate-radical leading to TC-degradation (see Section 3.2, Fig. 7, trace e). The ZnOvb is positioned at a more positive potential with respect to the couple OH-/·OH (+ 1.90 eV vs NHE) [60] and therefore presents the potential required for the generation of ·OH-radicals leading to TC-degradation.

4. Conclusions

The mechanism of photocatalysis still leaves many unanswered points related to the "hybrid" interactions of light with the local magnetized domains in the Fe-containing composites. The addition of FeO_x to ZnO extends the visible light absorption of the Ag_xO/ZnO NTs. Evidence is presented for the favorable effect of ZnO-FeOx intra-gap states compared to the $Ag_xO(15\%)/ZnO$ NTs during TC-degradation. By the use of appropriate $O_2^-\cdot$ and vbh$^+$ scavengers, it was possible to identify the ROS species leading to TC-degradation. Based on the potential band positions of ZnO and Ag_2O, an IFCT scheme is suggested for the interfacial charge transfer (IFCT) between Ag_2O and ZnO. Magnetic separation of the $Ag_xO(15\%)/FeO_x(20\%)/ZnO$ nanotubes after TC removal presents advantages over conventional processes reducing the cost of the photocatalyst separation from the suspension after TC-degradation.

Acknowledgements

Appendix A. Supplementary data

Supplementary material related to this article can be found, in the online version, at doi:https://doi.org/10.1016/j.apcatb.2019.02.046.

References

[1] P. Grenni, V. Ancona, A.B. Caracciolo, Ecological effects of antibiotics on natural ecosystems: a review, Microchem. J. 136 (2018) 25–39.
[2] S. Reardon, Antibiotic resistance sweeping developing world: bacteria are increasingly dodging extermination as drug availability outpaces regulation, Nature 509 (2014) 141–143.
[3] A.L. Ling, N.R. Pace, M.T. Hernandez, T.M. Lapara, Tetracycline resistance and class 1 integron genes associated with indoor and outdoor aerosols, Environ. Sci. Technol. 47 (2013) 4046–4052.
[4] Y. Chen, K. Liu, Preparation and characterization of nitrogen-doped TiO_2/diatomite integrated photocatalytic pellet for the adsorption-degradation of tetracycline hydrochloride using visible light, Chem. Eng. J. 302 (2016) 682–696.
[5] K. Kümmerer, Antibiotics in the aquatic environment. A review, Part I, Chemosphere 75 (2009) 417–434.

[6] R.A. Palominos, M.A. Mondaca, A. Giraldo, G. Peñuela, M. Pérez-Moya, H.D. Mansilla, Photocatalytic oxidation of the antibiotic tetracycline on TiO₂ and ZnO suspensions, Cat. Today 144 (2009) 100–105.

[7] I. Dalmázio, M.O. Almeida, R. Augusti, T.M.A. Alves, Monitoring the degradation of tetracycline by ozone in aqueous medium via atmospheric pressure ionization mass spectrometry, J. Am. Soc. Mass. Spectr. 18 (2007) 679–687.

[8] P.A. Blackwell, H.C.H. Lützhof, H.P. Ma, Ultrasonic extraction of veterinary antibiotics from soils and pig slurry with SPE clean-up and LC-UV and fluorescence detection, Talanta 64 (2004) 1058–1064.

[9] Y. Gao, Y. Li, L. Zhang, H. Huang, J. Hu, M. Shah, X. Su, X, Adsorption and removal of tetracycline antibiotics from aqueous solution by graphene oxide, J. Colloid Interf. Sci. 368 (2012) 540–546.

[10] G.H. Safari, M. Hoseini, M. Seyedsalehi, H. Kamani, J. Jaafari, A.H. Mahvi, Photocatalytic degradation of tetracycline using nanosized titanium dioxide in aqueous solution, Int. J. Environ. Sci. Technol. (Tehran) 12 (2015) 603–616.

[11] N. Chong, B. Jin, C.W.K. Chow, C. Saint, Recent developments in photocatalytic water treatment technology: a review, Water Res. 44 (2010) 2997–3027.

[12] R. Hao, X. Xiao, X. Zuo, J. Nan, W. Zhang, Efficient adsorption and visible-light photocatalytic degradation of tetracycline hydrochloride using mesoporous BiOI microspheres, J. Hazard. Mat. 209 (2012) 137–145.

[13] A. Kolodziejczak-Radzimska, T. Jesionowski, Zinc Oxide, From synthesis to applications: a review, Materials 7 (2014) 2833–2881.

[14] D. Segets, J. Gradl, R.K. Taylor, V. Vassilev, W. Peukert, Analysis of optical absorbance spectra for the determination of ZnO nanoparticle size distribution, solubility and surface energy, ACS Nano 3 (2009) 1703–1710.

[15] F. Pan, C. Song, X. Liu, Y. Fang, F. Zeng, Ferromagnetism and possible applications in spintronics of transition-metal-doped ZnO films, Mat. Sci. Eng. Res. 62 (2008) 1–35.

[16] D. Chu, Y. Masuda, T. Ohji, K. Kato, Formation and photocatalytic application of ZnO nanotubes using aqueous solution, Langmuir 26 (2009) 2811–2815.

[17] H. Lu, H. Li, L. Liao, Y. Tian, M. Shuai, J. Li, P. Zhu, Low-temperature synthesis and photocatalytic properties of ZnO nanotubes by thermal oxidation of Zn nanowires, Nanotechnology 19 (2008) 045605.

[18] Q. Yu, W. Fu, C. Yu, H. Yang, R. Wei, M. Li, S. Liu, Y. Sui, Z. Liu, M. Yuan, G. Zou, G. Wang, C. Shao, Y. Liu, Fabrication and optical properties of large-scale ZnO nanotube bundles via a simple solution route, J. Phys. Chem. C 111 (2007) 17521–17526.

[19] Y. Chen, H. Zhao, B. Liu, H. Yang, Charge separation between wurtzite ZnO polar {001} surfaces and their enhanced photocatalytic activity, Appl. Catal. B 163 (2015) 189–197.

[20] H. Wang, G. Li, L. Jia, G. Wang, C. Tang, Controllable preferential-etching synthesis and photocatalytic activity of porous ZnO nanotubes, J. Phys. Chem. C 112 (2008) 11738–11743.

[21] R. Chen, Ch. Zou, J. Bian, A. Sandhu, W. Gao, Microstructure and optical properties of Ag-doped ZnO nanostructures prepared by a wet oxidation doping process, Nanotechnology 22 (2011) 105706.

[22] M. Meng, Y. Li, Y. Lai, F. Yu, One-step synthesis, characterizations and mechanistic study of nano-sheets constructed fluffy ZnO and Ag/ZnO spheres used for Rhodamine B photo-degradation, Appl. Catal. B 100 (2010) 491–501.

[23] J. Yu, D. Sun, T. Wang, F. Li, Fabrication of Ag@ AgClZnO submicron wire film catalyst on glass substrate with excellent visible light photocatalytic activity and reusability, Chem. Eng. J. 334 (2018) 225–236.

[24] S. Zhao, Z. Cheng, L. Kang, M. Li, Z. Gao, The facile preparation of Ag decorated TiO₂/ZnO nanotubes and their potent photocatalytic degradation efficiency, RSC Adv. 7 (2017) 50064–50071.

[25] J. Zhang, X. Liu, L. Wang, T. Yang, X. Guo, S. Wu, S. Wang, S. Zhang, Synthesis and gas sensing properties of α-Fe₂O₃@ZnO core-shell nano-spindles, Nanotechnology 22 (2011) 185501.

[26] F. Wang, J. Liu, X. Wang, J. Kong, S. Qiu, G. Lu, C. He, Alpha-Fe₂O₃@ZnO heterostructured nanotubes for gas sensing, Mater. Lett. 76 (2012) 159–161.

[27] Y. Liu, L. Sun, J. Wu, T. Fang, R. Cai, A. Wei, Preparation and photocatalytic activity of ZnO/Fe₂O₃ nanotube composites, Mat. Sci. Eng. B 194 (2015) 9–13.

[28] S. Das, S. Sinha, B. Day, R. Jayabalan, M. Suar, A. Mishra, A. Tamhankar, C. Lundborg, S. Tripathy, Disinfection of multidrug resistant *Escherichia coli* by solar-photocatalysis using Fe-doped ZnO nanoparticles, Sci. Repts. 7 (2017) 104.

[29] A. Amarjargal, L.D. Tijing, I.T. Im, C.S. Kim, Simultaneous preparation of Ag/Fe₃O₄ core-shell nanocomposites with enhanced magnetic moment and strong antibacterial and catalytic properties, Chem. Eng. J. 226 (2013) 243–254.

[30] G. Mamba, J. Kiwi, C. Pulgarin, R. Sanjines, S. Giannakis, S. Rtimi, Evidence for the degradation of an emerging pollutant by a mechanism involving iso-energetic charge transfer under visible light, Appl. Catal. B 233 (2018) 175–183.

[31] J.P. Nogier, M. Delamar, X-ray photoelectron spectroscopy of TiO₂/V₂O₅ catalysts, Catal. Today 20 (1994) 109–123.

[32] J.F. Moulder, W.F. Stickle, P.E. Sobol, K.D. Bomben, J. Chastain (Eds.), Handbook of X-Ray Photoelectron Spectroscopy, Perkin-Elmer Corporation (Physical Electronics Division), Minnesota, USA, 1992.

[33] D.A. Shirley, High-resolution X-ray photoemission spectrum of the valence bands of gold, Phys. Rev. B 5 (1972) 4709–4714.

[34] M. Mangayayam, J. Kiwi, S. Giannakis, C. Pulgarin, I. Zivkovic, A. Magrez, S. Rtimi, FeOx magnetization enhancing *E. coli* inactivation by orders of magnitude on Ag-TiO₂ nanotubes under sunlight, Appl. Catal. B 202 (2016) 438–445.

[35] Z.H. Shah, J. Wang, Y. Ge, C. Wang, W. Mao, S. Zhang, R. Lu, Highly enhanced plasmonic photocatalytic activity of Ag/Ag/Cl/TiO₂ by CuO co-catalyst, J. Mater. Chem. 3 (2015) 3568–3575.

[36] A. Mahmood, S.M. Ramay, Y.S. Al-Zaghaer, M. Imran, S. Atiq, M.S. Al-Johany, Magnetic and photocatalytic response of Ag-doped ZnFeO nanocomposites for photocatalytic degradation of reactive dyes in aqueous solution, J. Alloys Compounds 614 (2014) 436–442.

[37] I. Matai, A. Sachdev, P. Dubey, S.U. Kumar, B. Bhushhan, P. Gopinath, Antibacterial activity and mechanism of Ag/ZnO nanocomposites on *S. Aureus* and GFP-expressing antibiotic resistant *E. Coli*, Colloids Surf. B: Bio-interfaces 115 (2014) 359–367.

[38] K.L. Hardee, A.J. Bard, Photo-electrochemical behavior of several polycrystalline metal oxide electrodes in aqueous solutions, J. Electrochem. Soc. 124 (1977) 215–224.

[39] H. Yousaf, H.M. Rafique, M. Amin, S.M. Ramay, S. Atiq, N.S. Alzayed, S.A. Siddiqi, Visible light induced Fe-doped magnetic photocatalyst nanoparticles for the degradation of methylene blue, J. Nanomater. Biostruct. 12 (2017) 91–98.

[40] E. Viollier, P.W. Inglett, K. Hunter, A.N. Roychoudhury, P. Van Cappellen, The ferrozine method revisited: Fe(II)/Fe(III) determination in natural waters, Appl. Geochem. 15 (200) 785-790.

[41] V. Nadtocheko, J. Kiwi, Primary photochemical reactions of the photo-feton system with ferric chloride, Environ. Sci. Technol. 32 (1998) 3273–3281.

[42] G.A. Parks, The isoelectric points of solid oxides, solid hydroxydes and aqueous hydroxo-complex systems, Chem. Revs. 65 (1965) 177–198.

[43] E. Topoglidis, E. Palomares, Y. Astuti, A. Green, C.J. Campbell, J.R. Durrant, Immobilization and electrochemistry of negatively charged proteins and modified crystalline metal oxide electrodes, Electrocatalysis 17 (2005) 1035–1041.

[44] S. Jiao, S. Zheng, D. Yin, L. Wang, L. Chen, Aqueous photolysis of tetracycline and toxicity of photolytic products to luminescent bacteria, Chemosphere 73 (2008) 377–382.

[45] G. Mamba, C. Pulgarin, J. Kiwi, M. Bensimon, S. Rtimi, Synchronic coupling of Cu₂O(p)/CuO(n) semiconductors leading to Norfloxacin degradation under visible light: kinetics, mechanism and film surface properties, J. Catal. 353 (2017) 133–140.

[46] B.D. Cullity, Elements of X-ray Diffraction, Addison-Wesley Pub. Co, Reading, Mass, 1986.

[47] X.Q. Wei, B.Y. Man, M. Liu, C.S. Xue, H.Z. Zhuang, C.Yang, Blue luminescent centers and microstructural evaluation by XPS and Raman in ZnO thin films annealed in vacuum, N₂ and O₂, Phys. B: Condens. Matter 388 (2007) 145–152.

[48] T.Bora L. Laxman, S. Dobrestov, J. Dutta, Defect engineered visible light active ZnO nanorods for photocatalytic treatment of water, Catal. Today 284 (2017) 11–18.

[49] J. Wang, Z. Wang, B. Huang, Y. Ma, Y. Liu, X. Qin, X. Zhang, Y. Dai, Oxygen vacancy induced band-gap narrowing and enhanced visible light photocatalytic activity of ZnO, ACS Appl. Mater. Interface 4 (2012) 4024–4030.

[50] L.A. Peyser, A.E. Vinson, A.P. Bartko, R.M. Dickson, Photo-activated fluorescence from individual silver nanoclusters, Science 291 (2001) 103–106.

[51] R. Feynman, R. Leighton, M. Sands, Feynman Lectures on Physics, Addison-Wesley, USA, 2005.

[52] C. O'Luanaigh, New Results Indicate That the New Particle Is a Higgs Boson, CERN, 2013 -10-09.

[53] N. Bohr, Resonance in nuclear photo-effects, Nature 141 (1938) 1096–1097.

[54] A. Einstein, N. Rosen, The particle problem in the general theory of relativity, Phys. Rev. 48 (1933) 73–77.

[55] Nonstoichiometry, Diffusion, and Electrical Conductivity in Binary Metal Oxides, Per Kofstad, Wiley-Interscience, 1972.

[56] X.X. Shang, T. Cao, Z. Lu, Y.C. Lin, F. Zhang, Y. Wang, Z. Li, J.C. Hone, J.A. Robinson, D. Smirnov, S.G. Louie, T.F. Heinz, Magnetic brightening and control of dark excitons in monolayer WSe₂, Mater. Sci. Eng. 12 (2017) 883–888.

[57] R.A. Smith, Semiconductors, 2ⁿᵈ edition, Cambridge University Press, Cambridge, New York, 1978, p. 532.

[58] A. Warshel, P.K. Sharma, M. Kato, Y. Xiang, H. Kiu, M. Olsson, Electrostatic basis for enzyme catalysis, Chem. Rev. 106 (2006) 3210–3235.

[59] P.V. Kamat, Boosting the efficiency of quantum dot sensitized solar cells through modulation of interfacial charge transfer, Acc. Chem. Res. 45 (2012) 1906–1915.

[60] B. Sulzberger, S. Canonica, T. Egli, W. Giger, J. Klausen, Urs von Gunten, Oxidative transformations of contaminants in natural and technical systems, Chimia 51 (1997) 900–907.